



OPEN

SUBJECT AREAS:

OPTOELECTRONIC
DEVICES AND
COMPONENTS

OPTICAL SENSORS

High performance organic-inorganic perovskite-optocoupler based on low-voltage and fast response perovskite compound photodetector

Dong Li, Guifang Dong, Wenzhe Li & Liduo Wang

Key Laboratory of Organic Optoelectronics and Molecular Engineering of Ministry of Education, Department of Chemistry, Tsinghua University, Beijing 100084, China.

Received
29 September 2014Accepted
18 December 2014Published
20 January 2015Correspondence and
requests for materials
should be addressed to
G.D. (donggf@mail.
tsinghua.edu.cn)

Organic-inorganic hybrid photodetectors attract considerable attention because they can combine the advantages of both organic and inorganic systems. Here, a perovskite compound with a broad absorption spectrum and high power conversion efficiency is used as a photosensitive layer in an organic/inorganic hybrid heterojunction photodetector with a high and fast response. The high sensitivity exceeding 10^4 is obtained at bias of 0–4 V. Using a tandem organic light-emitting diode (OLED) as the light source, we fabricated an optocoupler device. The optocoupler achieved a maximum photoresponsivity of 1.0 A W^{-1} at $341.3 \mu\text{Wcm}^{-2}$ at an input voltage of 6 V. The device also exhibits rapid response times of $\tau_{\text{rise}} \sim 20 \mu\text{s}$ and $\tau_{\text{fall}} \sim 17 \mu\text{s}$; as well as a high current transfer ratio (CTR) of 28.2%. After applying an amplification circuit, the CTR of the optocoupler increases to 263.3%, which is comparable with that of commercial inorganic optocouplers. The developed hybrid optocoupler thus shows great promise for use in photonics.

Optocouplers are important photoelectric devices with fine anti-jamming ability for noise control in signal communication and detection^{1–3}. Structurally, an optocoupler is composed of a light emitter as input and a photodetector (PD) as output. The input signal drives the light source and converts the electrical signal into an optical signal that is then reconverted into an electrical signal by the PD unit. Because the input and output are not common ground, potential fluctuation of the input does not affect the output potential, and the load fluctuation and noise of the output do not influence the input signal. Meanwhile, because an optocoupler transfers electrical signals using light in a coupling medium to prevent electrical contact of its input and output, it is also an excellent isolating device that can tolerate very large isolation voltages. For example, an optocoupler can control a high-potential circuit of several thousand volts using a low-potential signal of less than 10 V. Therefore, the optocoupler is an attractive prospect to realize both electrical isolation and signal conversion. However, as the most important part in optocouplers, most PDs must apply a certain operating voltage (1–100 V), which currently makes the overall circuitry of optocouplers uneconomical. Therefore, the ‘self-powered’ or ‘low-voltage’ PDs, which can generate built-in potential for their own operation and do not need a high external applied operating voltage, have attracted considerable attention⁴. Here, PDs with p-n or p-i-n junctions play an important role because they have superiorities in photosensitivity and frequency response characteristics, and more importantly, they can operate in photovoltaic mode without a high external operating bias^{5–7}.

Recently, with the development of organic materials, research on organic optoelectronic devices is burgeoning because of merits including low cost, low process temperature, ease of large-area fabrication and flexibility^{7,8}. However, these devices suffer from drawbacks such as relatively low carrier mobility and efficiency. The first polymer organic optocoupler (OOC) was reported in 1994 by Yu and Heeger⁹. The current transfer ratio (CTR) of this device was 0.2%. More recently, our group reported an OOC based on small molecules with a CTR of 0.17%². At present, the highest CTR of the OOC is 5.4%, which was achieved using a high-efficiency organic light-emitting diode (OLED) and bulk heterojunction organic PD¹⁰. On the other hand, inorganic PDs^{11,12} exhibit high carrier mobility and absorption compared with their organic counterparts, but they have disadvantages such as high fabricating temperature and low flexibility. Therefore, organic-inorganic hybrid-PDs that combine the advantages of both are desired^{4,13}.

Here, due to the broad absorption spectrum and high power-conversion efficiency^{14–21}, we use the perovskite compound as the photosensitive layer in an organic/inorganic hybrid heterojunction PD with a high and fast



response. Inorganic/organic perovskite compounds such as methylammonium lead iodide ($\text{CH}_3\text{NH}_3\text{PbI}_3$) have been widely used as light harvesters in solar cells^{14–19} because of their broad absorption spectrum and high carrier mobility²⁰. Due to their large short-circuit current density (16.5 mA cm^{-2}) and open-circuit voltage (0.997 V)¹⁴, hybrid PDs containing $\text{CH}_3\text{NH}_3\text{PbI}_3$ have great potential to produce optocouplers with large CTRs that can operate as ‘self-powered’ or at ‘low-voltage’. PDs with high responsivity and flexibility have been reported^{22,23}, however, they exhibited very slow response times of longer than 0.02 s , which limits their use in applications that require a rapid frequency-response.

Here, we report a fast-response perovskite-optocoupler based on a white tandem OLED light source and low-voltage organic/inorganic hybrid-PD using $\text{CH}_3\text{NH}_3\text{PbI}_3$ as a light harvester, p-type 2, 2', 7, 7'-tetrakis-(N,N-di-p-methoxyphenylamine)-9, 9'-bifluorene (spiro-MeOTAD) as a hole-transport material (HTM) and n-type mesoporous titania (mp-TiO₂). The device shows ‘self-power’ property operating at a zero-applied field, with a photoresponsivity of 284 mA W^{-1} at 0 V bias. The optocoupler device exhibits a maximum photoresponsivity of 1.0 A W^{-1} at $341.3 \text{ } \mu\text{Wcm}^{-2}$ ($V_{\text{OLED}} = 6 \text{ V}$) and 3.8 A W^{-1} at $15.9 \text{ } \mu\text{Wcm}^{-2}$ ($V_{\text{OLED}} = 5 \text{ V}$), which is higher than that of many commercial inorganic PDs²⁴. A maximum CTR of 28.2% is obtained, which is much higher than that of other OOCs reported. By adding an amplification circuit, the optocoupler exhibits a maximum CTR of 263.3%, comparable with the commercial inorganic ones (usually 50%–200%). The optocoupler also shows rapid frequency-response with the response time on the order of microseconds. The fast photoresponse and high photosensitivity of this low-voltage hybrid-PD, make it, as well as the perovskite-optocoupler, very promising candidates for practical use as photoelectric devices.

Results and Discussion

A $\text{CH}_3\text{NH}_3\text{PbI}_3$ film was prepared by spin-coating PbI_2 solution on the mp-TiO₂ substrate that was then dipped into $\text{CH}_3\text{NH}_3\text{I}$ solution. Figure 1a shows a cross-sectional micrograph of the $\text{CH}_3\text{NH}_3\text{PbI}_3$ PD device taken by a scanning electron microscope (SEM). It is apparent that the pores of mp-TiO₂ film are infiltrated with $\text{CH}_3\text{NH}_3\text{PbI}_3$. Figure 1b presents a surface SEM image of the $\text{CH}_3\text{NH}_3\text{PbI}_3$ overlayers on top of the mp-TiO₂ film. This image shows that several nanometre-sized $\text{CH}_3\text{NH}_3\text{PbI}_3$ islands form densely on top of mp-TiO₂ film. The $\text{CH}_3\text{NH}_3\text{PbI}_3$ domains do not appear to be continuous, however, there should be large contact areas for the interface between the $\text{CH}_3\text{NH}_3\text{PbI}_3$ and HTM overlayers, which should allow effective extraction of charge carriers to the electrode. The $\text{CH}_3\text{NH}_3\text{PbI}_3$ film coated on mp-TiO₂ was characterized by X-ray diffraction (XRD). The diffraction pattern of $\text{CH}_3\text{NH}_3\text{PbI}_3$ (Figure S1) contains peaks at 14.21° , 28.57° and 31.91° , corresponding to the (110), (220) and (310) planes, respectively. It confirms the formation of a tetragonal perovskite structure with lattice parameters of $a = b = 8.88 \text{ \AA}$ and $c = 12.68 \text{ \AA}$, which are consistent with previous reports^{15,16}.

Figure 1c depicts the schematic diagram of the device structure based on the SEM analysis (Figure 1a), and Figure 1d shows the corresponding energy level diagram. Under irradiation, when the light energy is larger than the bandgap of $\text{CH}_3\text{NH}_3\text{PbI}_3$, many excitons are photogenerated in the perovskite layer, and then dissociate at both the TiO₂/ $\text{CH}_3\text{NH}_3\text{PbI}_3$ and $\text{CH}_3\text{NH}_3\text{PbI}_3$ /HTM interfaces, because $\text{CH}_3\text{NH}_3\text{PbI}_3$ can act as both n- and p-type semiconductors¹⁴ and form junctions with different types of neighboring semiconductors. Besides, under an applied external electric field with the same direction as that of the built-in electric field at the heterojunction interface, the photogenerated excitons could also be sepa-

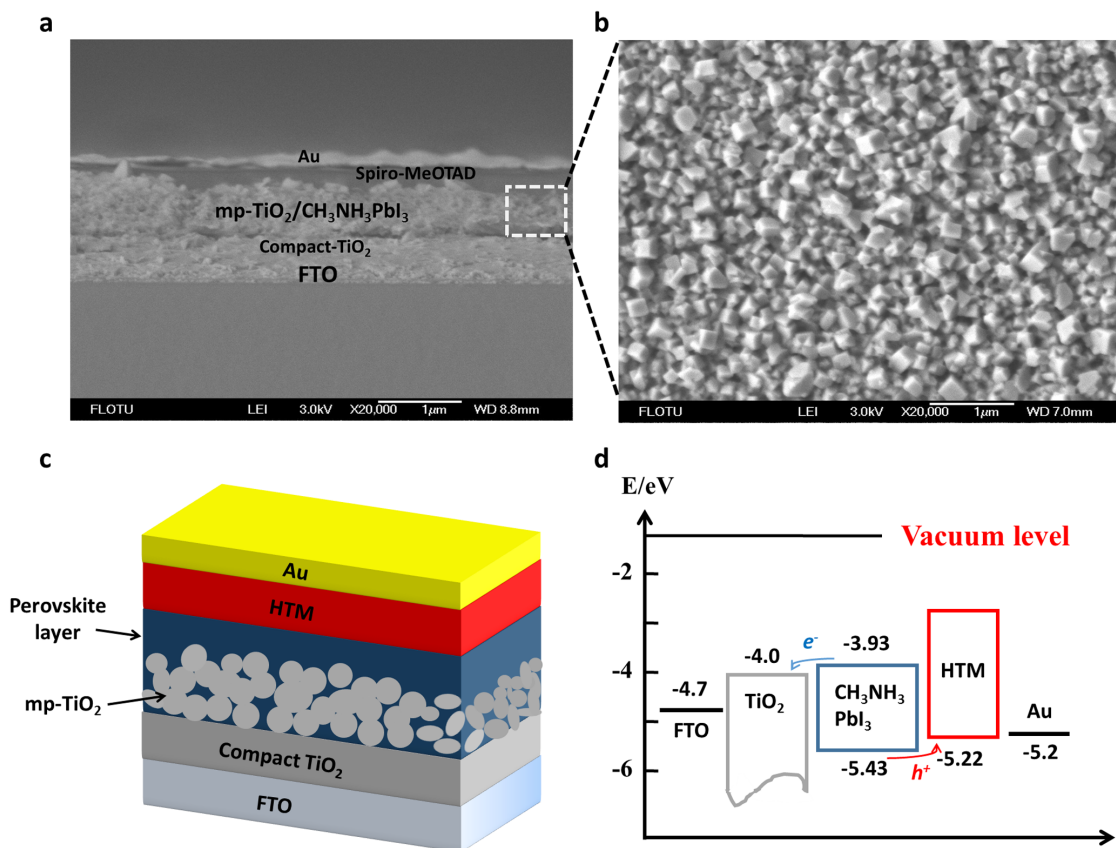


Figure 1 | Structure of the perovskite photodetector. (a) Cross-sectional SEM image of the $\text{CH}_3\text{NH}_3\text{PbI}_3$ PD. (b) SEM image of the surface of $\text{CH}_3\text{NH}_3\text{PbI}_3$ overlayers on top of mp-TiO₂ film. (c) Schematic diagram of the structure of the PD. (d) Energy level diagram of the PD.



rated in the $\text{CH}_3\text{NH}_3\text{PbI}_3$ layer, and then the photogenerated carriers can diffuse to the $\text{TiO}_2/\text{CH}_3\text{NH}_3\text{PbI}_3$ and $\text{CH}_3\text{NH}_3\text{PbI}_3/\text{HTM}$ interfaces. The lowest unoccupied molecular orbital (LUMO) level of $\text{CH}_3\text{NH}_3\text{PbI}_3$ (-3.93 eV) is higher than the conduction band energy level of TiO_2 (-4.0 eV) and the highest occupied molecular orbital (HOMO) level of $\text{CH}_3\text{NH}_3\text{PbI}_3$ (-5.43 eV) is lower than that of HTM (-5.22 eV) (Figure 1d), so the electrons are injected into the TiO_2 conduction band and simultaneously the holes are transferred to spiro-MeOTAD. It is clear that the favorable alignment of the energy levels of these semiconductors make them suitable candidates for PDs.

Further advantages of $\text{CH}_3\text{NH}_3\text{PbI}_3$ are that it exhibits a long electron lifetime and has a diffusion distance of nearly 500 nm (see Supplementary Information and Figure S2), which is much higher than that of most organic materials (usually less than 50 nm). The carrier lifetime measured by intensity modulated photovoltage spectroscopy (IMVS) was in the order of 10^{-3} s, which is much longer than that of many organic semiconductors (typically $10^{-7} \sim 10^{-4}$ s)^{25,26}. From the IMVS plot together with the intensity modulated photocurrent spectroscopy (IMPS) measurement, the electron diffusion distance has an average value of 405 nm. As we know, thick layers are generally used in devices to increase photon absorption, but the relatively short diffusion distance of most semiconductors can result in the recombination of many photogenerated carriers, which seriously limits the increase of photocurrent. Here, the long electron lifetime and diffusion distance of $\text{CH}_3\text{NH}_3\text{PbI}_3$ mean that most photogenerated carriers can be utilized to produce photocurrent. Therefore, we can effectively improve the light absorption and exciton dissociation, thereby improving the performance of this hybrid-PD.

We further investigated the spectral response and calculated the wavelength-dependent responsivity of the device from the external quantum efficiency (EQE) using the expression $R(\lambda) = \text{EQE}/h\nu$, where $h\nu$ is the energy of the incident photon in electron volts (eV). The absorption spectrum of $\text{CH}_3\text{NH}_3\text{PbI}_3$ and incident photon-to-electron conversion efficiency (IPCE) action spectrum of the perovskite device are shown in Figure 2. The device exhibits a broad photoresponse range from 400 to 750 nm, and maximum responsivity of 284 mA W^{-1} at 490 nm and 0 V PD bias, which is higher than some commercial PDs and previously reported self-powered ones^{4–6,12,13}. High photoresponse at 0 V bias is also obtained under the illumination with a solar simulator (Supplementary Information Figure S3). The different work functions of the electrodes (see Figure 1d) mean that there could be parasitic injection of holes and/or electrons from the electrodes^{27,28}, which may be why the minimum dark current is observed at ~ -0.5 V.

We coupled this perovskite hybrid-PD with an OLED to fabricate an organic-inorganic perovskite optocoupler (Figure 3a). Here, the OLED is the input component and the PD is the output component. CTR, the ratio of output current density to input current density, is the primary parameter to evaluate the efficiency of an optocoupler¹.

In general, CTR can be described as:

$$\text{CTR} = \frac{J_{\text{out}}}{J_{\text{in}}} = \int \eta_{\text{IQE}}^{\text{OLED}}(\lambda) \cdot \eta_{\text{out}}(\lambda) \cdot \eta_{\text{in}}(\lambda) \cdot \eta_{\text{IQE}}^{\text{PD}}(\lambda) d\lambda \quad (1)$$

where $\eta_{\text{IQE}}^{\text{OLED}}(\lambda)$ and $\eta_{\text{IQE}}^{\text{PD}}(\lambda)$ are the single wavelength internal quantum efficiency (IQE) of the OLED and PD at wavelength λ , respectively. $\eta_{\text{out}}(\lambda)$ is the outcoupling efficiency of the OLED, and $\eta_{\text{in}}(\lambda)$ is the incoupling efficiency of the PD.

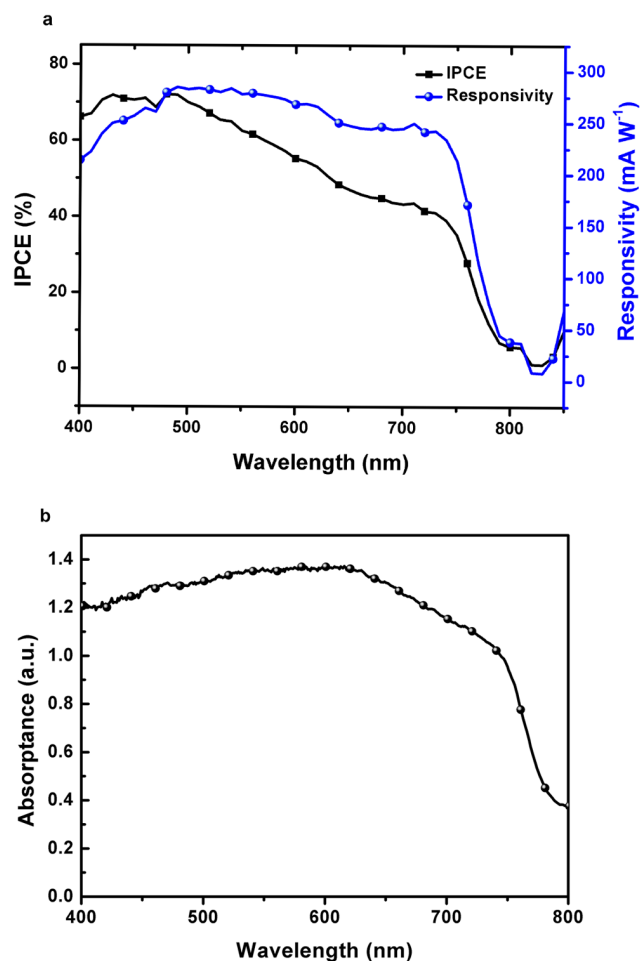


Figure 2 | Spectral properties of the perovskite photodetector. (a) IPCE spectrum and responsivity of the PD from 400 to 800 nm. (b) Absorption spectrum of the $\text{CH}_3\text{NH}_3\text{PbI}_3$ layer on top of mp- TiO_2 film.

From Equation (1), for the input component, two important factors should be taken into consideration to achieve a high CTR. The input component should have a high current efficiency (CDA), and its electroluminescence (EL) spectrum should match the absorption of the output component so that the output component obtains high responsivity (R). The absorption bands of $\text{CH}_3\text{NH}_3\text{PbI}_3$ are located in the visible region from 400 to 750 nm (Figure 2b), so a tandem white OLED with high current efficiency (44.0 cd A^{-1}) and EL spectrum from 470 to 650 nm (Figure S4) was used as the input component. The active layers of the input component were thermally evaporated sequentially and then encapsulated in N_2 (Supplementary Information).

We measured the current density (J)-voltage (V) characteristics of the output component under different input voltages (Figure S5a). A maximum photoresponse of 1.0 A W^{-1} at $341.3 \mu\text{Wcm}^{-2}$ ($V_{\text{input}} = 6$ V) was observed as shown in Figure 3b, and a photoresponse of 3.8 A W^{-1} was demonstrated at $15.9 \mu\text{Wcm}^{-2}$ ($V_{\text{input}} = 5$ V). The highest detectivity value of $3.29 \times 10^{12} \text{ cm Hz}^{0.5}\text{W}^{-1}$ (Jones) is obtained because of the high photocurrent and low dark current in this device (Figure S5b).

The output-voltage-dependence of the CTR is presented in Figure 3c. The maximum CTR is 28.2% at an output bias of 2–4 V and input bias of 6 V, which is much higher than that of reported OOC devices and comparable with that of inorganic ones^{10,29}. The transfer characteristics of the perovskite optocoupler are shown in Figure 3d. The output current density is observed to be proportional to the input current density over about three orders of magnitude,

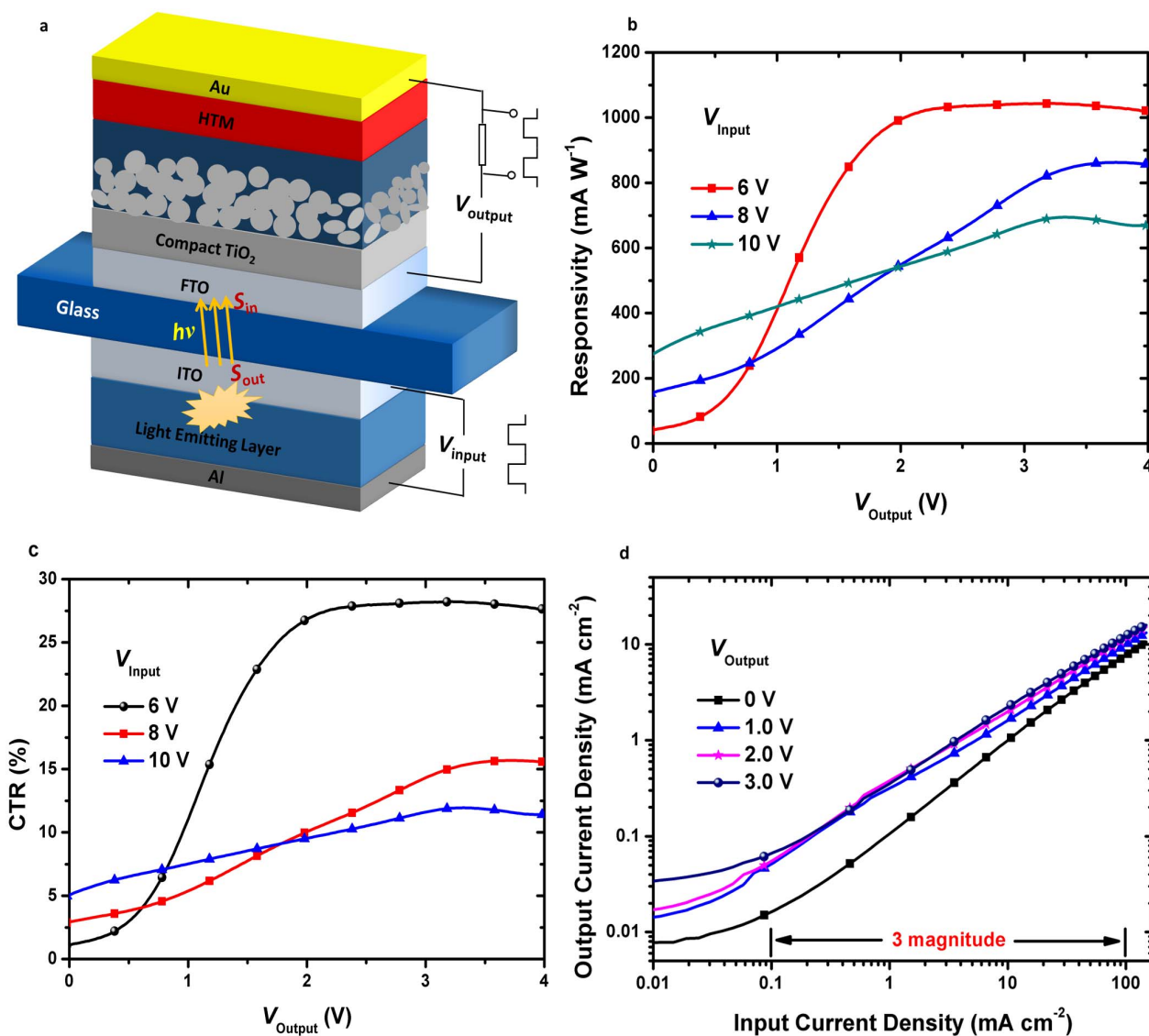


Figure 3 | Structure and properties of an organic/inorganic hybrid optocoupler. (a) Schematic diagram of the organic-inorganic hybrid optocoupler device with a tandem OLED as the input light source and a perovskite PD as the output component. (b) Responsivity of the $\text{CH}_3\text{NH}_3\text{PbI}_3$ perovskite PD under the illumination of the tandem OLED with different input voltages (and thus different light intensities). (c) CTR of the optocoupler device under different input OLED voltage and applied PD bias. (d) The output current density of the $\text{CH}_3\text{NH}_3\text{PbI}_3$ perovskite PD under different OLED input current densities. (The dots are a visual guide.)

suggesting that the perovskite optocoupler would be capable of working in analog circuits. After applying an amplification circuit in this optocoupler, a maximum CTR of 263.3% was obtained according to Figure 4. CTR is magnified by about 10 times at an applied bias of 3 V, while there is not any change in CTR at the applied bias of 0 V after inclusion of an amplification circuit because of the invalidation of the amplification circuit at zero bias.

Commercial inorganic optocouplers usually exhibit the CTR value of 50 ~ 200%, so this sort of perovskite optocoupler shows promise as an alternative to commercial inorganic optocouplers in the applications such as image sensors and low-voltage-control circuit in an intelligent robot³. These are the most important parts of a modern electrical control system, because they avoid operation risk and allow easy automation. Compared with commercial inorganic optocouplers, the perovskite optocoupler should have the superiorities in lower cost, lower process temperature, easier large-area fabrication and increased flexibility.

Response time is another significant parameter for high-speed optoelectronic applications. Figure 5 shows the frequency-response

characteristics of the optocoupler corresponding to response time at an input signal of 5 kHz. As designed, the phases of the output and input signals are opposite, which proves that the optical signal is successfully transported. The rise time (τ_{rise}) and fall time (τ_{fall}) are defined as the times taken by the signal to vary between 10% and 90% of the saturation value. With a square-wave voltage applied as the input signal and a constant voltage applied on output circuit, the amplitude attenuation could be read out under different input frequencies. A clear saturation is observed in the transient signal with $\tau_{\text{rise}} \sim 20 \mu\text{s}$ and $\tau_{\text{fall}} \sim 17 \mu\text{s}$ for a device area of 16 mm^2 . The cut-off frequency is 40 kHz and the output signal is capable of following the input signal at a modulation frequency of 200 kHz despite the phase delay (Figure S6b).

Conclusions

In summary, we developed a PD composed of $\text{CH}_3\text{NH}_3\text{PbI}_3$ with the advantages of low-voltage operation, fast response and broad absorption spectrum (from 400 to 750 nm). Combining this PD exhibiting high photoresponsivity (1.0 A W^{-1} @ $341.3 \mu\text{Wcm}^{-2}$)

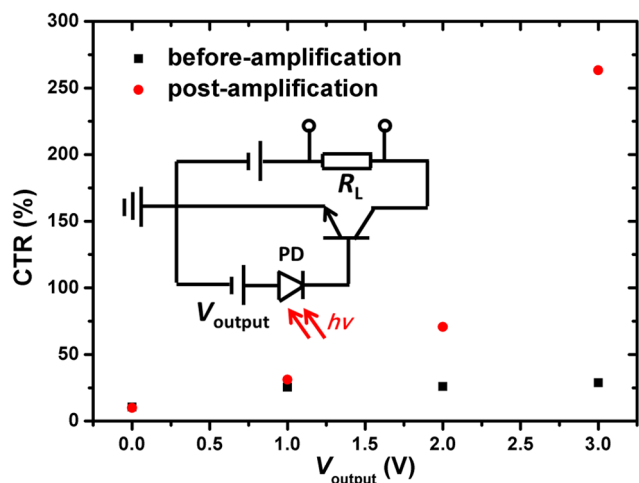


Figure 4 | Influence of an amplification circuit on the performance of the optocoupler. CTR of the optocoupler device under different applied PD bias with and without an amplification circuit. Inset: Circuit scheme of the optocoupler applying the amplification circuit.

with an efficient tandem white OLED, we fabricated an organic-inorganic hybrid perovskite optocoupler. Applying an amplification circuit in this optocoupler, we improve the CTR from 28.2% to 263.3%, which is comparable with that of commercial inorganic optocouplers. The optocoupler exhibited a rapid photoresponse with $\tau_{\text{rise}} \sim 20 \mu\text{s}$ and $\tau_{\text{fall}} \sim 17 \mu\text{s}$ for an area of 16 mm^2 . The cut-off frequency and maximum following frequency were 40 and 200 kHz, respectively. Our research demonstrates that perovskite optocouplers are attractive for use in high-efficiency, rapid-response photonics.

Methods

Materials preparation. Titanium (IV) isopropoxide ($\text{Ti}[\text{OCH}(\text{CH}_3)_2]_4$, 1 mL) was mixed with 2-methoxyethanol ($\text{CH}_3\text{OCH}_2\text{CH}_2\text{OH}$, 5 mL) and ethanolamine ($\text{H}_2\text{NCH}_2\text{CH}_2\text{OH}$, Aldrich, 99.8%, 0.5 mL) and then heated to 80°C for 2 h under magnetic stirring in a glove box. Nanocrystalline TiO_2 paste (18NRT) was purchased from Dyesol and diluted to w/w 33%. PbI_2 was purchased from Aldrich and dissolved in DMF to give a concentration of 462 mg mL^{-1} . The $\text{CH}_3\text{NH}_3\text{I}$ was dissolved in 2-propanol to give a concentration of 10 mg mL^{-1} . The HTM was prepared from a solution of Spiro-MeOTAD (73 mg), Li-TFSI (99.95%, Aldrich) in acetonitrile ($17.5 \mu\text{L}$, 520 mg mL^{-1}) and TBP (96%, Aldrich, $37.5 \mu\text{L}$) in chlorobenzene (99.8%, Aldrich, 1 mL).

Device fabrication. The TiO_2 precursor was spin coated on a cleaned fluorine-doped tin oxide (FTO) substrate at 3000 rpm for 30 s, and then heated at 500°C for 60 min to form a blocking layer. The nanocrystalline TiO_2 paste was deposited on the pre-treated

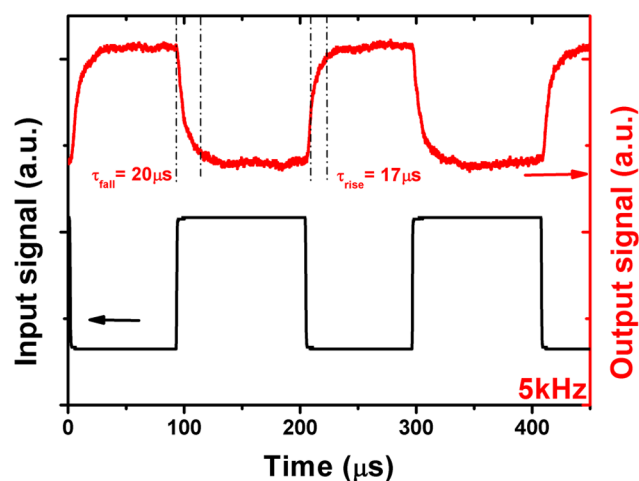


Figure 5 | Frequency response of the optocoupler. The frequency response of the optocoupler device under pulsating frequency of 5 kHz.

FTO substrate at 7000 rpm for 30 s, followed by heating at 500°C for 1 h. PbI_2 in DMF (Aldrich, 99.9%) was heated to 60°C for 2 h under magnetic stirring and then spin coated on the as-prepared TiO_2 film at 5000 rpm for 60 s in a glove box. The films were dried at 70°C for 30 min. Subsequently, the dried films were dipped into a solution of $\text{CH}_3\text{NH}_3\text{I}$ in for 120 s and rinsed with 2-propanol. The films were heated to 70°C for 30 min. The dark red $\text{CH}_3\text{NH}_3\text{PbI}_3$ -coated TiO_2 films were covered with HTM solution by spin-coating method at 4000 rpm for 30 s. 60 nm-thick Au counter electrode was deposited on the top of the HTM over layer by a thermal evaporation. The active area was fixed at $4 \times 4 \text{ mm}^2$. The thickness of TiO_2 , $\text{CH}_3\text{NH}_3\text{PbI}_3$ and HTM films was 500, 200, and 80 nm, respectively.

Characterization. The UV-vis absorption spectra were used for testing the absorption of perovskite sensitized TiO_2 film with an absorption spectrometer (Hitachi U-3010). XRD patterns were obtained with a diffractometer (Smart LAB instruments) using $\text{Cu K}\alpha$ beam ($\lambda = 1.54 \text{ \AA}$). The electrical characteristics were measured using a semiconductor parameter analyzer (Keithley 4200 Semiconducting System). And Thermo AM 1.5 Solar Simulator was used to measure the photosensitivity of PD. IPCE spectrum was measured by ZAHNER CIMPS electrochemical workstation, Germany. To test the frequency characteristic, an input square-wave voltage applied on the OLED was generated by a GFG-8016G function generator and the output signal of the photodiode was enlarged by an amplification circuit made by ourselves. The photodiode was inversely triggered at the falling edge of input signals to eliminate the disturbance of induced overshoot noise between input and output. The main body of the optocoupler was placed in a shielding box to isolate environmental noises. Real photocurrent signal was recorded by Tektronix DPO 4104 oscilloscope.

- Sun, Q. J., Dong, G. F., Wang, L. D. & Qiu, Y. Organic optocouplers. *Sci China Chem* **54**, 1017–1026 (2011).
- Dong, G. F., Zheng, H. Y., Duan, L., Wang, L. D. & Qiu, Y. High-Performance Organic Optocouplers Based on a Photosensitive Interfacial C_{60}/NPB Heterojunction. *Adv Mater* **21**, 2501–2504 (2009).
- Li, D. *et al.* A flexible blue light sensitive organic photodiode with high properties for the applications in low-voltage-control circuit and flexion sensors. *Laser Photonics Rev* **8**, 316–323 (2014).
- Game, O., Singh, U., Kumari, T., Banpurkar, A. & Ogale, S. ZnO(N)-Spiro-MeOTAD hybrid photodiode: an efficient self-powered fast-response UV (visible) photosensor. *Nanoscale* **6**, 503–513 (2014).
- Bie, Y. Q. *et al.* Self-Powered, Ultrafast, Visible-Blind UV Detection and Optical Logical Operation based on ZnO/GaN Nanoscale p-n Junctions. *Adv Mater* **23**, 649–653 (2011).
- Wu, D. *et al.* Self-powered and fast-speed photodetectors based on CdS:Ga nanoribbon/Au Schottky diodes. *J Mater Chem* **22**, 23272–23276 (2012).
- Li, L. S., Huang, Y. Y., Peng, J. B., Cao, Y. & Peng, X. B. Highly responsive organic near-infrared photodetectors based on a porphyrin small molecule. *J Mater Chem C* **2**, 1372–1375 (2014).
- Lee, K. H. *et al.* Green-Sensitive Organic Photodetectors with High Sensitivity and Spectral Selectivity Using Subphthalocyanine Derivatives. *ACS Appl Mater Inter* **5**, 13089–13095 (2013).
- Yu, G., Pakbaz, K. & Heeger, A. J. Optocoupler Made from Semiconducting Polymers. *J Electron Mater* **23**, 925–928 (1994).
- Yang, D. Z., Sun, H. D., Chen, J. S. & Ma, D. G. High Current Transfer Ratio Organic Optocoupler Based on Tandem Organic Light-Emitting Diode as the Input Unit. *Chinese Phys Lett* **29**, 114216 (2012).
- Fang, X. S. *et al.* An Efficient Way to Assemble ZnS Nanobelts as Ultraviolet-Light Sensors with Enhanced Photocurrent and Stability. *Adv Funct Mater* **20**, 500–508 (2010).
- Gao, Z. W. *et al.* Self-powered flexible and transparent photovoltaic detectors based on CdSe nanobelt/graphene Schottky junctions. *Nanoscale* **5**, 5576–5581 (2013).
- Xie, Y. R. *et al.* Self-powered solid-state photodetector based on TiO_2 nanorod/spiro-MeOTAD heterojunction. *Appl Phys Lett* **103**, 261109 (2013).
- Heo, J. H. *et al.* Efficient inorganic-organic hybrid heterojunction solar cells containing perovskite compound and polymeric hole conductors. *Nat Photonics* **7**, 487–492 (2013).
- Malinkiewicz, O. *et al.* Perovskite solar cells employing organic charge-transport layers. *Nat Photonics* **8**, 128–132 (2014).
- Liu, D. Y. & Kelly, T. L. Perovskite solar cells with a planar heterojunction structure prepared using room-temperature solution processing techniques. *Nat Photonics* **8**, 133–138 (2014).
- Lee, M. M., Teuscher, J., Miyasaka, T., Murakami, T. N. & Snaith, H. J. Efficient Hybrid Solar Cells Based on Meso-Superstructured Organometal Halide Perovskites. *Science* **338**, 643–647 (2012).
- Noh, J. H., Im, S. H., Heo, J. H., Mandal, T. N. & Seok, S. I. Chemical Management for Colorful, Efficient, and Stable Inorganic-Organic Hybrid Nanostructured Solar Cells. *Nano Lett* **13**, 1764–1769 (2013).
- Ball, J. M., Lee, M. M., Hey, A. & Snaith, H. J. Low-temperature processed meso-superstructured thin-film perovskite solar cells. *Energ Environ Sci* **6**, 1739–1743 (2013).
- Stoumpos, C. C., Malliakas, C. D. & Kanatzidis, M. G. Semiconducting Tin and Lead Iodide Perovskites with Organic Cations: Phase Transitions, High



- Mobilities, and Near-Infrared Photoluminescent Properties. *Inorg Chem* **52**, 9019–9038 (2013).
21. Burschka, J. *et al.* Sequential deposition as a route to high-performance perovskite-sensitized solar cells. *Nature* **499**, 316–319 (2013).
 22. Xia, H. R., Li, J., Sun, W. T. & Peng, L. M. Organohalide lead perovskite based photodetectors with much enhanced performance. *Chem Commun* **50**, 13695–13697 (2014).
 23. Hu, X. *et al.* High-Performance Flexible Broadband Photodetector Based on Organolead Halide Perovskite. *Adv Funct Mater* DOI: 10.1002/adfm.201402020 (2014).
 24. Wu, S. H. *et al.* Visible-blind ultraviolet sensitive photodiode with high responsivity and long term stability. *Appl Phys Lett* **97**, 023306 (2010).
 25. Credgington, D. & Durrant, J. R. Insights from Transient Optoelectronic Analyses on the Open-Circuit Voltage of Organic Solar Cells. *J Phys Chem Lett* **3**, 1465–1478 (2012).
 26. Maurano, A. *et al.* Recombination Dynamics as a Key Determinant of Open Circuit Voltage in Organic Bulk Heterojunction Solar Cells: A Comparison of Four Different Donor Polymers. *Adv Mater* **22**, 4987–4992 (2010).
 27. Saracco, E. *et al.* Work Function Tuning for High-Performance Solution-Processed Organic Photodetectors with Inverted Structure. *Adv Mater* **25**, 6534–6538 (2013).
 28. Sakai, J., Taima, T. & Saito, K. Efficient oligothiophene: fullerene bulk heterojunction organic photovoltaic cells. *Org Electron* **9**, 582–590 (2008).
 29. Yao, Y., Chen, H. Y., Huang, J. S. & Yang, Y. Low voltage and fast speed all-polymeric optocouplers. *Appl Phys Lett* **90**, 253103 (2007).

Acknowledgments

This work was financially supported by the National Natural Science Foundation of China (No. 61177023, 61474069 and 51273104).

Author contributions

L.D.W. conceived and designed the experiments. D.L. and W.Z.L. contributed equally to perform the experiments. W.Z.L. helped with the sample preparation. D.L., W.Z.L. and G.F.D. contributed to data analysis. G.F.D., D.L. and L.D.W. wrote the manuscript. All authors discussed the results and commented on the paper.

Additional information

Supplementary information accompanies this paper at <http://www.nature.com/scientificreports>

Competing financial interests: The authors declare no competing financial interests.

How to cite this article: Li, D., Dong, G., Li, W. & Wang, L. High performance organic-inorganic perovskite-optocoupler based on low-voltage and fast response perovskite compound photodetector. *Sci. Rep.* **5**, 7902; DOI:10.1038/srep07902 (2015).



This work is licensed under a Creative Commons Attribution-NonCommercial-ShareAlike 4.0 International License. The images or other third party material in this article are included in the article's Creative Commons license, unless indicated otherwise in the credit line; if the material is not included under the Creative Commons license, users will need to obtain permission from the license holder in order to reproduce the material. To view a copy of this license, visit <http://creativecommons.org/licenses/by-nc-sa/4.0/>